Corrosion Science 123 (2017) 21–26

Contents lists available at ScienceDirect

Corrosion Science

journal homepage: www.elsevier.com/locate/corsci

Transition from superhydrophilic to superhydrophobic state of laser textured stainless steel surface and its effect on corrosion resistance

Uroš Trdan[a,*], Matej Hočevar[b], Peter Gregorčič[a]

[a] Faculty of Mechanical Engineering, University of Ljubljana, Aškerčeva 6, 1000 Ljubljana, Slovenia
[b] Institute of Metals and Technology, Lepi pot 11, 1000 Ljubljana, Slovenia

ARTICLE INFO

Keywords:
A. Stainless steel
B. Polarization
B. SEM
C. Intergranular corrosion
C. Passivity
C. Pitting corrosion

ABSTRACT

This work investigates the evolution from superhydrophilic to superhydrophobic surface state on corrosion behaviour of SS316L produced by Nd:YAG nanosecond direct laser texturing (DLT). Results confirm perfect correlation among wettability and corrosion, hence superhydrophobic surface with a contact angle of 168 ± 3.0° reflects in enhanced passivity, lower anodic dissolution and corrosion current reduction. Characterization of the corrosion attack by 3D microscopy reveals high sensitivity of superhydrophilic surfaces on corrosion propagation direction in regard to the laser beam passage (90°/0°). However, this trend completely diminishes with superhydrophobic development. Further, DLT also completely prohibits intergranular corrosion detected with the non-processed sample.

1. Introduction

Recently, intensive research efforts have been devoted to synthesize lotus-like, superhydrophobic, surfaces with water contact angle in excess of 150° and sliding angle below 5° [1,2]. Such functionalized surfaces possess several unique beneficial properties, i.e. extreme water repellency [3,4], self-healing [5], self-cleaning [6], reduced drag in laminar and turbulent flows [7,8], enhanced heat transfer [9,10] and improved corrosion resistance [11–17].

Artificial super-hydrophobic surfaces have been successfully fabricated via various chemical methods, such as plasma and chemical etching, anodic oxidization, chemical vapor deposition, sol–gel method, etc. [11,15,16,18]. Nonetheless, in recent years laser surface texturing has emerged as a novel, versatile, clean and low waste nanotechnology for producing multi-modal surfaces with micro/nano structure due to laser ablation and melting [2,5,7,19]. Emelyanenko et al. [5] fabricated a superhydrophobic surface on 321H AISI stainless steel. Their results have confirmed extreme water repellency with excellent functional durability under prolonged abrasive wear and cavitation loads. Ta et al. [20] demonstrated that superhydrophobic surfaces on SS304 with steady contact angle of 154° and contact angle hysteresis of 4° can be fabricated via direct laser texturing (DLT) with cost-effective, compact nanosecond fiber laser system. Further, it has been shown [3,14] that nanosecond laser texturing of various Al alloys can greatly improve resistance to localized corrosion attack in a sodium chloride solution due to multimodal roughness with μ-cavities consisting of air entrapment hence preventing penetration of corrosive species at solution/metal interface.

However, despite considerable progress in this area, little attention has been paid to investigate transition from superhydrophilic to superhydrophobic effect on corrosion behaviour of laser textured stainless steel surface along with the influence of laser passage direction (90°/0°). Hence, the aim of this work is to study how the evolution of hydrophobicity, i.e. water repellency of direct laser textured (DLT) SS316L influences corrosion behaviour in an aggressive 0.6 M NaCl solution. Specific attention was focused on the collateral influence of bimodal surface topography to the initiation and propagation of corrosion.

2. Material and methods

2.1. Laser texturing

We textured surfaces of AISI 316L stainless steel samples with the following chemical composition (in wt.%): Cr 16.9, Ni 10.04, Mo 2.07, Mn 1.84, Si 0.57, Cu 0.41, P 0.036, C 0.019, S 0.0009, V 0.077, Nb 0.015, N 0.044, and Fe the rest. Commercial 1 mm thick sheet of AISI 316L alloy was cut in samples with diameter of 15 mm and textured by using a marking nanosecond Nd:YAG pulsed laser (LPKF, OK DP10) with a wavelength of 1064 nm, pulse duration of 40 ns (FWHM), pulse frequency of 25 kHz, and pulse energy of 0.22 mJ. A scanning head (Scanlab SCANgine 14) with an F-Theta focusing lens was used for

* Corresponding author.
E-mail addresses: uros.trdan@fs.uni-lj.si (U. Trdan), matej.hocevar@imt.si (M. Hočevar), peter.gregorcic@fs.uni-lj.si (P. Gregorčič).

http://dx.doi.org/10.1016/j.corsci.2017.04.005
Received 3 January 2017; Received in revised form 9 April 2017; Accepted 11 April 2017
Available online 18 April 2017
0010-938X/

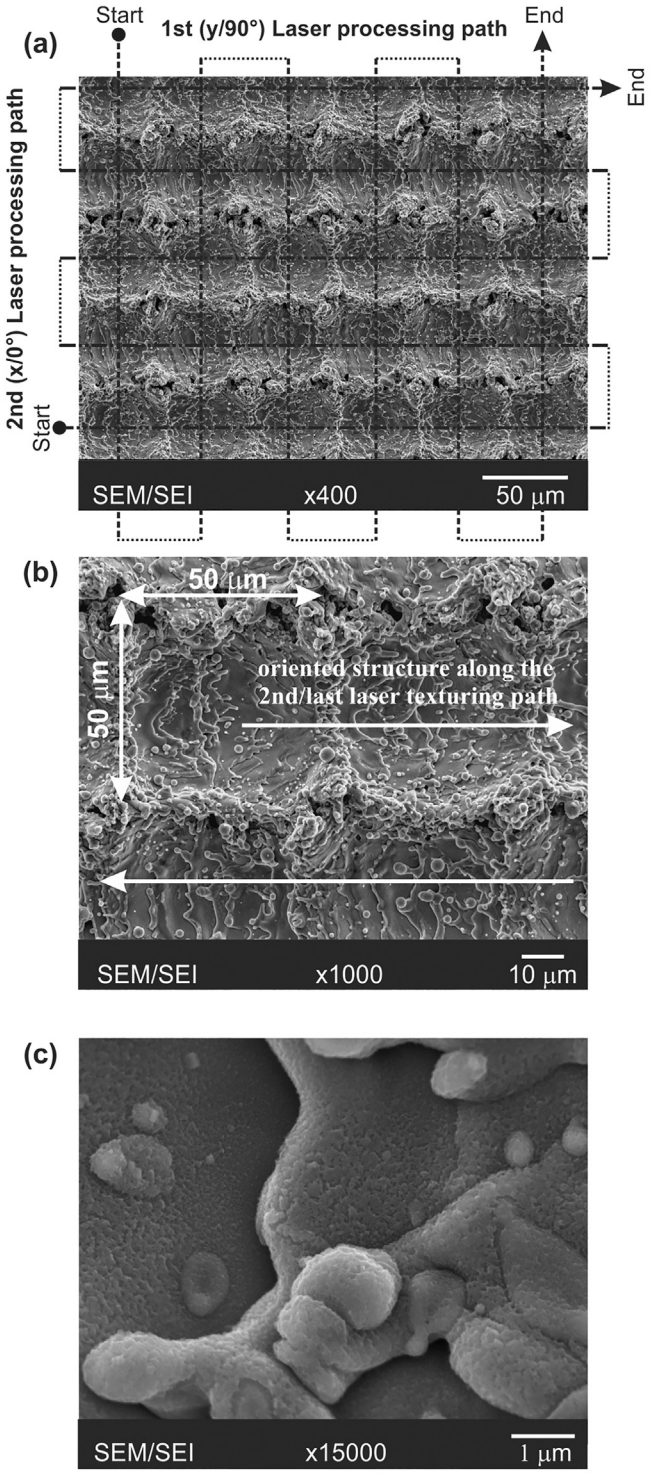

Fig. 1. SEM micrographs of laser textured surfaces.

delivery of a focused laser beam over the sample surface with beam spot diameter of 0.03 mm and a constant speed of 150 mm/s, first in the y (90°) and then in the x (0°) direction (e.g., see dashed lines in Fig. 1a). The distance between adjacent laser scanning lines − the so-called scan line separation − equalled 50 µm in both directions. Before processing, all samples were ultrasonically cleaned in distilled water for 12 min and rinsed by ethanol.

2.2. Surface morphology and wettability measurements

Surface morphology of untreated and laser textured samples prior to and after corrosion experiments were examined by a non-contact Alicona G4 3D optical Infinite-Focus Measuring (IFM) device and JEOL JSM-6500F scanning electron microscope (SEM). Evolution from superhydrophilic to superhydrophobic state of laser textured samples was examined by static contact angle θ measurements using a goniometer of our own design. Here, a droplet with volume of 5 µL distilled water was delivered to the investigated surface.

The transition from superhydrophilic to superhydrophobic state and its influence on corrosion behaviour was studied by using 4 samples (DLT#1-4), textured by same laser parameters, but exposed to ambient conditions (T = 25 °C, RH = 35%) for different time periods after laser texturing, i.e. 30 min (DLT#1), 24 h (DLT#2), 11 days (DLT#3) and 1 month (DLT#4), respectively. Before the transfer of samples to the electrolytic cell for corrosion experiments the contact angle measurements were performed and after that the samples were ultrasonically degreased in ethanol and rinsed in deionised water for 3 min each.

2.3. Electrochemical measurements

Electrochemical measurements were carried out with a PAR 263A potentiostat/galvanostat using a three-electrode component corrosion cell under static conditions. A saturated calomel electrode was used as a reference, graphite rod as a counter electrode along with the sample embedded in a Teflon PAR holder as the working electrode (1 cm^2). Test medium was a naturally aerated (pH = 6.8 ± 0.2; T = 23 ± 1 °C) 0.6 M NaCl solution prepared with deionised water.

Corrosion was tested using linear polarization resistance (LPR) and cyclic polarization (CP) electrochemical techniques. Before LPR and CP experiments open circuit potential measurements ($E_{ocp} = f[t]$) was performed for 60 min in order to stabilize the surface, whereas corrosion potential E_{corr}, was determined at the end of the stabilization process. LPR measurements were performed in the potential range ± 10 mV relative to E_{corr} using 0.1 mV/s potential scan rate. CP scans were performed with a scan rate of 1 mV/s, started at −250 mV vs. E_{corr} and increased in anodic direction up to 600 mV_{SCE}. Afterwards, the polarization direction was reversed and progressed in cathodic direction to the starting potential. All electrochemical corrosion techniques were pre-tested to ensure the repeatability of the experiments.

3. Results and discussion

3.1. The effect of laser texturing on surface morphology

Surface morphology of DLT sample (Fig. 1) clearly indicates the structuring effect due to laser irradiation. As shown in Fig. 1a multi-directional structure due to different laser scanning directions (90°/0°) is well pronounced. The µ-nets have 50 µm spacing corresponding to the scan line separation. The oriented structure along the second (last) laser texturing passage (Fig. 1b) indicates its primary solidification path (from left to right and vice versa) of the ablated/molten material. Further, SEM image at higher magnification (Fig. 1c) reveals multi-modal oriented structures as a consequence of constant melting, ablation and deposition of the recast material during laser texturing.

In order to evaluate the influence of DLT on the surface topography and roughness in both the vertical (y) and horizontal (x) directions of laser-beam scan an optical 3D microscope was used. Fig. 2 shows the 3D topography of laser textured surface, where the distinctive influence of the second laser texturing path can be observed. Further, µ-channels are completely opened and parallel to the last laser scanning direction and closed to the opposite direction (first laser scanning direction).

The roughness parameters obtained along valleys (x_1, y_1) and crests (x_2, y_2) of the specific direction in regards to the first (e.g., see y_1 and y_2 lines in Fig. 2) and second (e.g., see x_1 and x_2 lines in Fig. 2) scan lines path are listed in Table 1.

As can be seen from the results, roughness values parallel to the first

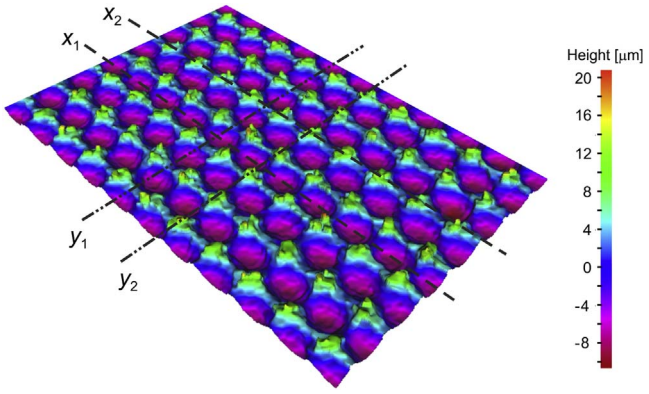

Fig. 2. 3D surface topography of laser textured surface with schematic presentation of the line roughness measurements along the first laser scan (y_1 and y_2) and the second laser scan x (x_1 and x_2).

Table 1
Roughness parameters values in specific directions marked on Fig. 2.

Parameter	*y1*	*y2*	*x1*	*x2*
R_a [µm]	3.20 ± 0.04	4.06 ± 0.15	2.15 ± 0.13	2.37 ± 0.07
R_q [µm]	3.67 ± 0.03	4.45 ± 0.14	2.44 ± 0.14	2.84 ± 0.10
R_z[µm]	13.4 ± 0.36	15.7 ± 0.62	8.62 ± 0.60	12.9 ± 0.80
S_a[µm]	4.62 ± 0.15			

laser beam passage reflects in much higher values compared to those obtained in parallel to the second scanning direction. For example, the roughness R_a achieved the minimum value of 2.15 ± 0.13 µm along valleys of the µ-channels (x_1) produced during the second texturing path, whereas in the opposite direction (y_1) it equals 3.20 ± 0.04 µm due to the metal ejection at the edges produced during the second DLT path. Similar trend was also obtained along crests, but with higher values of all roughness parameters in the first, i.e., *y* direction of laser passage path through the treated surface. Nonetheless, 5 separated measurements of 3D amplitude parameter on different DLT samples have confirmed good surface uniformity with an average S_a value of 4.62 ± 0.15 µm. For comparison, the non-processed sample achieved around 26 times lower S_a roughness with a value of 0.175 ± 0.02 µm.

3.2. Surface wettability development

The corrosion resistance of metals depends on several parameters, such as homogeneity and stability of the passive film, microstructural properties as well as surface roughness and wettability. Although, intrinsic wetting properties, namely, improves wetting for hydrophilic surfaces and increases the contact angle for hydrophobic ones, the influence of roughness on sensitivity to localized corrosion attack is very complex and sometimes for rough hydrophobic materials this sensitivity might be higher than for smooth surface [11,14]. To examine the isolated influence of wettability on corrosion behaviour we used the inherent property of laser textured metal surface, where a transition from hydrophilic to hydrophobic state appears if such a surface is exposed to the air at room conditions [11,12,21]. During this process the surface roughness on microscale stays the same.

The contact angle of non-processed and non-polished surface (as received sample, just ultrasonically cleaned in distilled water and rinsed by ethanol) equals 95.0 ± 6.4°, while the Young angle of the base material, measured on highly polished surface (R_a = 25 ± 2 nm) as suggested in ref. [22,23] equals θ_Y = 81.6 ± 5.7°. Immediately after laser texturing the surface experiences a super-hydrophilic state with a contact angle θ = 0°, i.e., the water forms a thin film covering the whole sample. At this time the surface is in a saturated state [24] of a Wenzel regime [25], where the roughness gains the wettability of a base material. The hydrophilic behaviour immediately after texturing is additionally increased also due to metal oxides appearing on the surface. When the textured surface is exposed to air at ambient conditions, the hydrophobicity is developed [11,12]. In our case, the contact angle increased to θ = 109 ± 6.7° in 11 days, while the superhydrophobic state in a Cassie-Baxter regime [26] with θ = 168 ± 3.0° and sliding angle below 3° was achieved in 1 month. After superhydrophobicity was developed, the contact angle appeared stable by time.

Several mechanisms contributing to this transition in ambient air over time have been proposed by different authors, i.e. decomposition of carbon dioxide into carbon with active magnetite [21], airborne hydrocarbon contamination and the absorption of organic matters from the atmosphere [27,28], partial surface deoxidation [29] and the creation of hydrophobic functional groups [30]. However, it should be noted that the mechanisms responsible for hydrophilic-to-hydrophobic transition after DLT is still under debate [27] and there is still not fully accepted theory to explain this behaviour.

Nevertheless, our results, i.e., the achieved contact angles of superhydrophobic surface and the time period needed for development of stable superhydrophobicity, are very similar to the results obtained by other authors, who used nanosecond lasers without any additional surface treatment [31,32]. We, therefore, studied how this − experimentally observed − transition influences the corrosion behaviour.

3.3. Linear polarization resistance (LPR) measurements

LPR measurements were performed after one hour's immersion at open circuit in the potential range ± 10 mV relative to E_{corr} using 0.1 mV/s scan rate. The corresponding values of polarization resistance R_p, determined from the slope of *E–i* curves [R_p = (d*E*/d*i*)] are given in Table 2.

The lowest R_p value in a 0.6 M NaCl solution was confirmed for the superhydrophilic samples DLT#1 & DLT#2, which achieved a value of 2.34 ± 0.15 kΩ cm^2 and 13.37 ± 0.86 kΩ cm^2, respectively. Both of

Table 2
Characteristic results derived from contact angle measurements and electrochemical measurements of non-processed and DLT processed samples exposed to ambient conditions for different time periods: R_p from LPR, and E_{corr}, E_{pit}, E_{rp} and i_{corr} from CP curves.

Parameter	Sample/Condition				
	Non-processed SS316L	DLT#1 (after 30 min)	DLT#2 (after 1 day)	DLT#3 (after 11 days)	DLT#4 (after 1 month)
θ [°]	95 ± 6.4	0 (saturated)	0 (saturated)	109 ± 6.7	168 ± 3.0
R_p [kΩ cm^2]	67.57 ± 5.25	2.34 ± 0.15	13.37 ± 0.86	80.04 ± 4.70	94.24 ± 4.16
E_{corr} [mV$_{SCE}$]	−175 ± 8	−321 ± 12	−212 ± 18	−98 ± 14	−162 ± 9
E_{pit} [mV$_{SCE}$]	18 ± 9	−66 ± 5	−51 ± 7	−4 ± 3	219 ± 11
E_{rp} [mV$_{SCE}$]	−195 ± 4	−316 ± 3	−214 ± 6	−159 ± 4	−197 ± 7
β_a [mV/dec]	330 ± 13	271 ± 16	330 ± 29	178 ± 15	269 ± 11
β_c [mV/dec]	−169 ± 8	−159 ± 20	−102 ± 11	−93 ± 6	−81 ± 9
i_{corr} [µA/cm^2]	0.72 ± 0.07	18.61 ± 2.26	2.53 ± 0.32	0.33 ± 0.02	0.29 ± 0.03

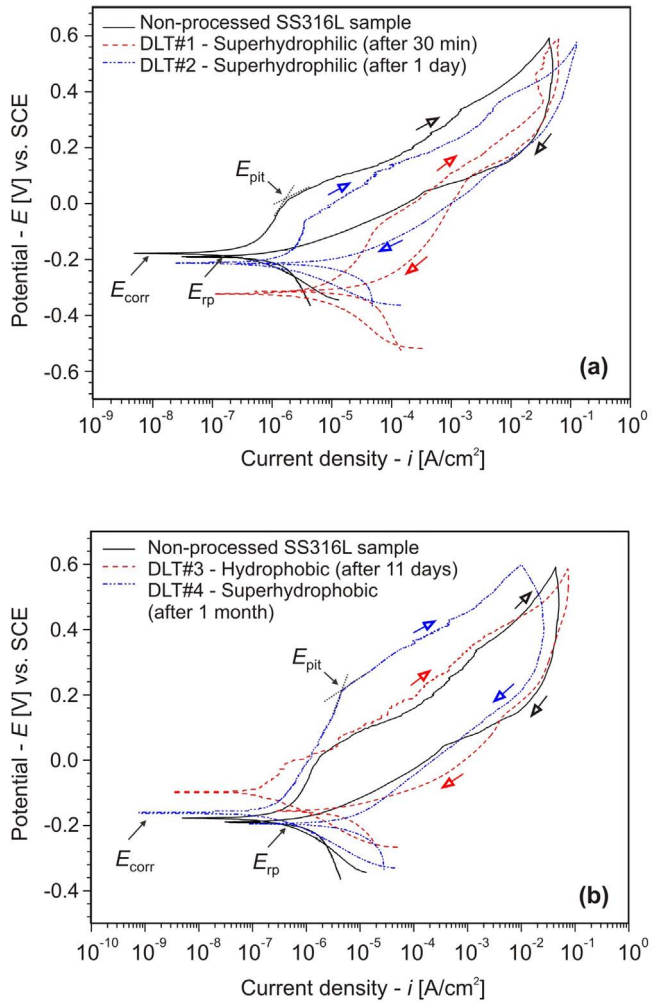

Fig. 3. Cyclic polarization (CP) curves in 0.6 M NaCl solution of non-processed SS316L sample compared to (a) DLT superhydrophilic samples and (b) DLT hydrophobic/superhydrophobic samples.

these samples indicate lower corrosion resistance to uniform corrosion, compared to the non-processed/base 316L steel sample, which reached a value of 67.57 ± 5.25 kΩ cm^2. However, with hydrophobic and superhydrophobic state R_p increases to 80.04 ± 4.70 kΩ cm^2 and 94.24 ± 4.16 kΩ cm^2, indicating enhanced resistance to the transfer of electrons to electro-active species in chloride environment [33].

3.4. Cyclic polarization (CP) measurements

CP curves of non-processed SS316L and DLT samples are shown in Fig. 3a and b. All CP curves show typical active/passive behaviour in the forward (anodic) scan. Afterwards, a sharp increase in anodic current due to a stable pit growth or pit propagation at pitting potential E_{pit} is observed with a well-defined hysteresis in the reverse, i.e. cathodic scan. Further, no distinct primary passivation potential was detected, which is typical for stainless steel materials.

The various characteristic potentials such as E_{corr}, E_{pit}, and E_{rp} obtained from the CP curves in a 0.6 M NaCl solution are presented in Table 2. The pitting potential (E_{pit}), at which a protective passive film is damaged as a result of pit initiation followed by pit propagation, was determined with extrapolation to the potential at which the current abruptly increases in the forward anodic scan. On the other hand, the repassivation/protection potential (E_{rp}) where pits or crevices repassivate, was determined as the potential at which the curve in reverse scan intersects the curve in forward scan [34]. The current density i_{corr} in μA/cm^2 was calculated according to the Stern–Geary equation:

$$i_{corr} = \frac{\beta_a \cdot \beta_c}{2.303 \cdot R_p \cdot (\beta_c - \beta_a)} \quad (1)$$

where R_p [kΩ cm^2] is polarization resistance (determined from the LPR test) and β_a and β_c are the anodic and cathodic Tafel constants (in mV/dec) determined by the Tafel extrapolation method.

Experimental results presented in Fig. 3 and Table 2 confirms the tremendous effect of the surface state of direct laser textured 316L stainless steel on corrosion behaviour. From the CP scans it is clearly understood that DLT in the superhydrophilic state has inferior corrosion resistance, compared with the base material. On the contrary, laser processed samples with developed hydrophobic/superhydrophobic state indicate superior corrosion resistance compared to the non-processed sample. A distinctive shift of the pitting potential can be noticed with the DLT#4 superhydrophobic sample (θ = 168 ± 3.0°), which was exposed to the ambient condition for 1 month. Here, E_{pit} is located at 219 ± 11 mV$_{SCE}$, which is 201 mV more positive than with the non-processed 316L stainless steel sample, suggesting that pitting corrosion is unlikely to occur.

Further, the analysis of characteristic potentials obtained from the CP curves shows that among all the samples, the DLT#4 exhibits the highest passivity ($E_{pit} - E_{corr}$) with lowest anodic dissolution in the transpassive region. Moreover, the calculated values of i_{corr} confirm good accordance with the LPR measurements, indicating importance of transition from superhydrophilic to superhydrophobic state on the corrosion behaviour. Thus, i_{corr} values indicate the following order of the corrosion resistance: DLT #1 (18.61 ± 2.26 μA/cm^2) < DLT#2 (2.53 ± 0.32 μA/cm^2) < non-processed 316L (0.72 ± 0.07 μA/cm^2) < DLT#3 (0.33 ± 0.02 μA/cm^2) < DLT#4 (0.29 ± 0.03 μA/cm^2).

3.5. Influence of wettability development on corrosion propagation

3D surface morphology after CP corrosion tests with the insert of wettability evolution (the contact angle measurement) are shown in Fig. 4. The corrosion without any preferred direction is developed on non-processed surface (Fig. 4a). Contrarily, the 3D measurement of corroded hydrophilic surface (Fig. 4b) clearly reveals high dependence of the corrosion attack propagating inside μ-channels produced during the last laser beam passage, despite the fact that the lowest roughness was obtained along the valleys of these channels (see Fig. 2 and Table 1). This phenomenon can be explained by an opened μ-channel along the last laser scanning direction and barriers in the perpendicular direction (see Fig. 2). However, the development of superhydrophobicity reduces the preferred direction of corrosion propagation, as clearly visible from Fig. 4c–d.

With superhydrophobic state developed, this effect is completely eradicated, since in this case the μ-channel along the last laser scanning direction does not act anymore as a channel for microfluidic. Instead, the developed superhydrophobicity increases a trapping air and reduces the fractional area of liquid–solid interface, as suggested by the Cassie-Baxter's model [26]. Another possible effect contributing to improved corrosion resistance is a grain refinement of the top surface layer due sequential cycles of melting/rapid cooling and quenching during DLT [17,35]. Gupta et al. [36] reported significantly improved pitting and oxidation resistance due to greater Cr diffusion and ease of formation of compact Cr-oxide layer resistance of nanocrystalline surface compared to the conventional coarse grained 316L SS surface. Such hierarchical super-hydrophobic structure with entrapped air acts as an effective corrosion resistant coating thus making the penetration of water molecules and halide ($C\bar{l}$) ions adsorption to the surface more difficult [3,11,14].

Fig. 5 shows surface condition after the CP tests of non-processed and laser textured superhydrophilic sample (DLT#1), respectively.

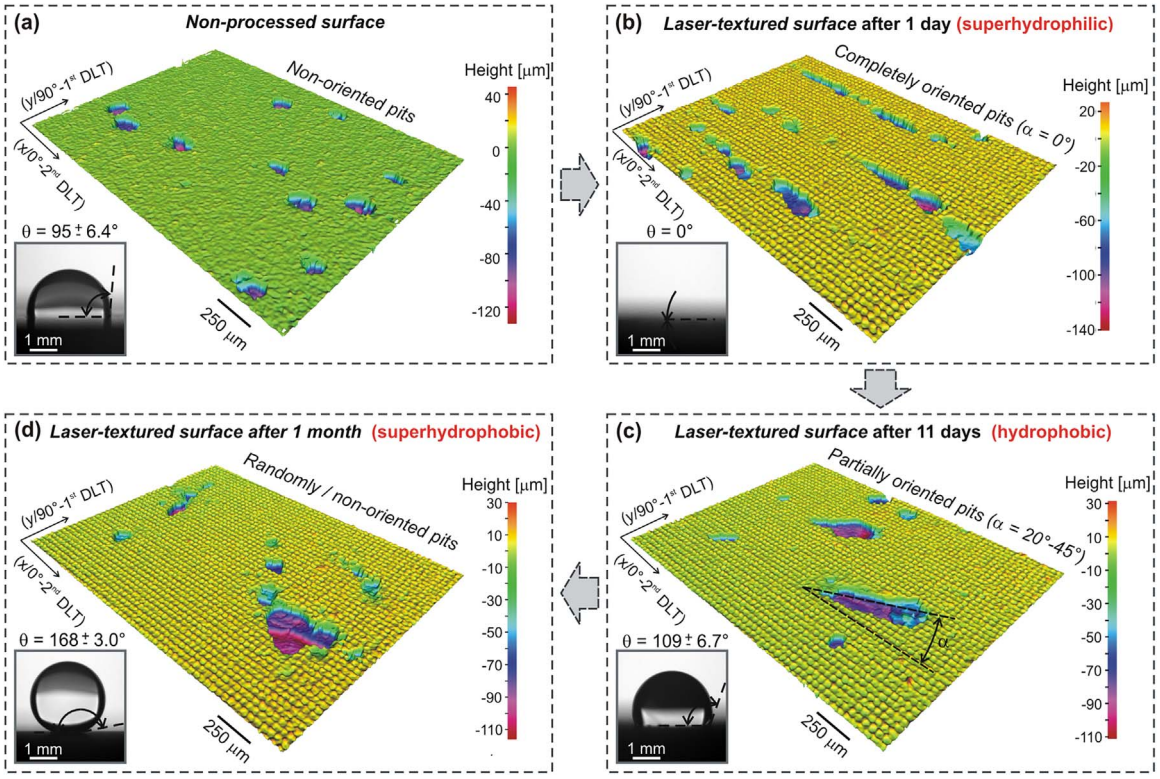

Fig. 4. 3D surface morphology after CP tests in a 0.6 M NaCl aqueous solution of (a) non-processed surface; and surfaces experienced the transition from (b) superhydrophilic (c) through hydrophobic to (d) superhydrophobic state.

Although, both SEM images confirms pitting attack in the form of spherical/non-oriented pits with the base sample and completely oriented pits with DLT#1 sample, only the base/non-processed sample exhibited intergranular corrosion (IGC) attack. This is an additional important benefit of DLT process, since austenitic chromium-nickel (300 series) stainless steels are prone to IGC in the proximity of chromium rich carbides [37]. The precipitation of Cr-rich $M(Fe,Cr)_{23}C_6$ carbides at grain boundaries often leads to the appearance of Cr-depleted zones that are prone to corrosion [38]. Since these precipitates are nobler than the adjacent boundary the galvanic effect promotes the anodic dissolution of the more negative grain boundaries acting as the continuous anodes [39]. This is an important factor, since after the occurrence of IGC attack, the corrosion resistance and mechanical properties of the stainless steels are drastically reduced.

In contrast, as can be seen in Fig. 5b, laser texturing completely prevents IGC attack, even in superhydrophilic state. This phenomenon is most likely attributed to more homogeneous microstructure with smaller amount of galvanic cells inside the material as a consequence of melting and deposition of the recast material due to laser texturing. Similar results were reported previously also by other authors [35,36]. For example, Kwok et al. [35] confirmed complete elimination of Cr-rich carbide phases in various austenitic SS samples due to laser surface melting process. Double loop electrochemical potentiokinetic reactivation (DL-EPR) tests in 0.5 M H_2SO_4 and 0.01 M KSCN solution have confirmed considerably higher resistance to IGC attack after laser surface melting as a result of more homogenous microstructure and the redissolution of Cr-rich carbides.

4. Conclusions

Direct laser texturing (DLT) using a nanosecond Nd:YAG laser was confirmed as an effective method for fabrication of superhydrophobic surfaces on 316L stainless steel. It was shown that the transition from superhydrophilic (θ = 0°) through hydrophobic (θ = 109 ± 6.7°) to superhydrophobic (θ = 168 ± 3.0°) state occurs due to exposure of the textured surface to ambient conditions, which enables examination

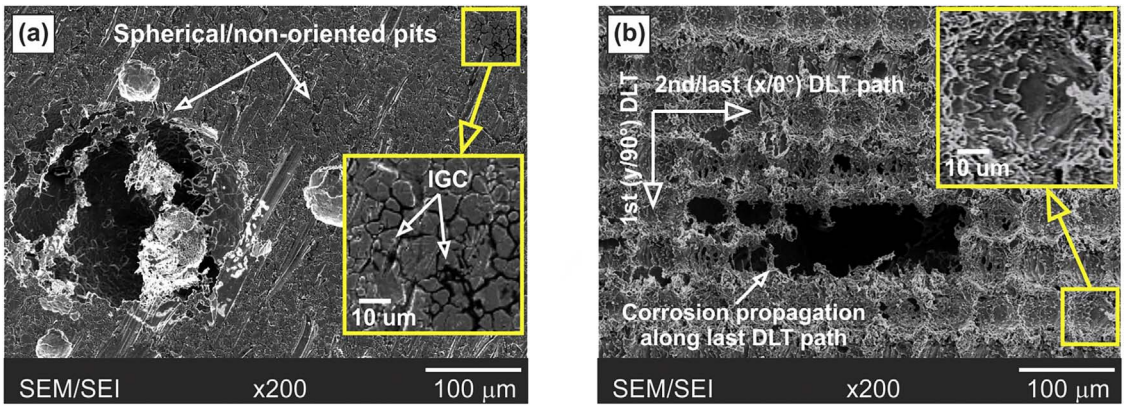

Fig. 5. SEM images after CP measurements. (a) Base/non-processed 316L sample and (b) DLT#1 superhydrophilic sample.

of the isolated influence of wettability on corrosion behaviour.

LPR and CP results confirmed perfect correlation with the development of water repellency. The highest corrosion resistance with the highest polarization resistance (R_p = 94.24 ± 4.16 kΩcm^2), improved passivation ability, and lowest corrosion current density (i_{corr} = 0.29 ± 0.03 μA/cm^2) was measured on the superhydrophobic sample. The electrochemical measurements clearly demonstrate that both the hydrophobic and superhydrophobic surface experience lower corrosion activity as the non-processed surface with 26 times lower roughness. Improved corrosion resistance is directly associated with entrapped air inside hierarchical hydrophobic structure, which reduces the fractional area of liquid–solid interface which makes the penetration of corrosive species to the surface more difficult.

Further, the 3D topography of superhydrophilic surface after corrosion test revealed a strong preferential direction of corrosion propagation along μ-channels that are oriented along the last texturing passage (0°). However, this effect is significantly reduced by development of water repellency, resulting in non-oriented pitting attack. More importantly, presented results indicate that laser texturing completely inhibits the initiation of inter-granular corrosion as a consequence of more homogeneous microstructure with smaller amount of galvanic cells, i.e. Cr-depleted grain boundaries/M(Fe,Cr)$_{23}$C$_6$ carbides.

Acknowledgment

The authors acknowledge the financial support from the state budget by the Slovenian Research Agency (Programme Nos. P2-0392, P2-0132 and P2-0270).

References

[1] F.A. Muller, C. Kunz, S. Graf, Bio-inspired functional surfaces based on laser-induced periodic surface structures, Materials 9 (476) (2016) 1–29.
[2] A.Y. Vorobyev, C.L. Guo, Direct femtosecond laser surface nano/microstructuring and its applications, Laser Photon. Rev. 7 (2013) 385–407.
[3] L. Ruiz de Lara, R. Jagdheesh, J.L. Ocaña, Corrosion resistance of laser patterned ultrahydrophobic aluminium surface, Mater. Lett. 184 (2016) 100–110.
[4] T. Liu, Y. Yin, S. Chen, X. Chang, S. Cheng, Super-hydrophobic surfaces improve corrosion resistance of copper in seawater, Electrochim. Acta 52 (2007) 3709–3713.
[5] A.M. Emelyanenko, F.M. Shagieva, A.G. Domantovsky, L.B. Boinovich, Nanosecond laser micro- and nanotexturing for the design of a superhydrophobic coating robust against long-term contact with water cavitation, and abrasion, Appl. Surf. Sci. 332 (2015) 513–517.
[6] O.U. Nimittrakoolchai, S. Supothina, Deposition of organic-based superhydrophobic films for anti-adhesion and self-cleaning applications, J. Eur. Ceram. Soc. 28 (2008) 947–952.
[7] M.A. Samaha, H.V. Tafreshi, M. Gad-el-Hak, Superhydrophobic surfaces: from the lotus leaf to the submarine, C. R. Mecan. 340 (2012) 18–34.
[8] A. Busse, N.D. Sandham, G. McHale, M.I. Newton, Change in drag, apparent slip and optimum air layer thickness for laminar flow over an idealised superhydrophobic surface, J. Fluid Mech. 727 (2013) 488–508.
[9] M. Zupančič, M. Steinbücher, P. Gregorčič, I. Golobič, Enhanced pool-boiling heat transfer on laser-made hydrophobic/superhydrophilic polydimethylsiloxane-silica patterned surfaces, Appl. Therm. Eng. 91 (2015) 288–297.
[10] M. Zupančič, M. Može, P. Gregorčič, I. Golobič, Nanosecond laser texturing of uniformly and non-uniformly wettable micro structured metal surfaces for enhanced boiling heat transfer, Appl. Surf. Sci. 399 (2017) 480–490.
[11] S. Khorsand, K. Raeissi, F. Ashrafizadeh, Corrosion resistance and long-term durability of super-hydrophobic nickel film prepared by electrodeposition process, Appl. Surf. Sci. 305 (2014) 498–505.
[12] L.B. Boinovich, S.V. Gnedenkov, D.A. Alpysbaeva, V.S. Egorkin, A.M. Emelyanenko, S.L. Sinebryukhov, A.K. Zaretskaya, Corrosion resistance of composite coatings on low-carbon steel containing hydrophobic and superhydrophobic layers in combination with oxide sublayers, Corros. Sci. 55 (2012) 238–245.
[13] Jianyi Kong Shi, Xingdong Wang, Xuewu Li, Preparation of multifunctional Al-Mg alloy surface with hierarchical micro/nanostructures by selective chemical etching processes, Appl. Surf. Sci. 389 (2016) 335–343.
[14] L.B. Boinovich, A.M. Emelyanenko, A.D. Modestov, A.G. Domantovsky, K.A. Emelyanenko, Synergistic effect of superhydrophobicity and oxidized layers on corrosion resistance of aluminum alloy surface textured by nanosecond laser treatment, ACS Appl. Mater. Interfaces 7 (2015) 19500–19508.
[15] W. Liu, Q.J. Xu, J. Han, X.H. Chen, Y.L. Min, A novel combination approach for the preparation of superhydrophobic surface on copper and the consequent corrosion resistance, Corros. Sci. 110 (2016) 105–113.
[16] H. Jie, Q.J. Xu, L. Wei, Y.L. Min, Etching and heating treatment combined approach for superhydrophobic surface on brass substrates and the consequent corrosion resistance, Corros. Sci. 102 (2016) 251–258.
[17] L.B. Boinovich, A.M. Emelyanenko, A.D. Modestov, A.G. Domantovsky, A.A. Shiryaev, K.A. Emelyanenko, O.V. Dvoretskaya, A.A. Ganne, Corrosion behavior of superhydrophobic aluminum alloy in concentrated potassium halide solutions: when the specific anion effect is manifested, Corros. Sci. 112 (2016) 517–527.
[18] T. Darmanin, E.T. de Givenchy, S. Amigoni, F. Guittard, Superhydrophobic surfaces by electrochemical processes, Adv. Mater. 25 (2013) 1378–1394.
[19] V.D. Ta, A. Dunn, T.J. Wasley, J. Li, R.W. Kay, J. Stringer, P.J. Smith, E. Esenturk, C. Connaughton, J.D. Shephard, Laser textured surface gradients, Appl. Surf. Sci. 371 (2016) 583–589.
[20] V.D. Ta, A. Dunn, T.J. Wasley, J. Li, R.W. Kay, J. Stringer, P.J. Smith, E. Esenturk, C. Connaughton, J.D. Shephard, Laser textured superhydrophobic surfaces and their applications for homogeneous spot deposition, Appl. Surf. Sci. 365 (2016) 153–159.
[21] A.M. Kietzig, S.G. Hatzikiriakos, P. Englezos, Patterned superhydrophobic metallic surfaces, Langmuir 25 (2009) 4821–4827.
[22] A. Marmur, Soft contact: measurement and interpretation of contact angles, Soft Matter. 2 (2006) 12–17.
[23] A. Sarkar, A.M. Kietzig, General equation of wettability: a tool to calculate the contact angle for a rough surface, Chem. Phys. Lett 574 (2013) 106–111.
[24] G. McHale, N.J. Shirtcliffe, M.I. Newton, Super-hydrophobic and super-wetting surfaces: analytical potential, Analyst 129 (2004) 284–287.
[25] R.N. Wenzel, Resistance of solid surfaces to wetting by water, Ind. Eng. Chem. 28 (1936) 988–994.
[26] A.B.D. Cassie, S. Baxter, Wettability of porous surfaces, Trans. Faraday Soc. 40 (1944) 0546–0550.
[27] L.B. Boinovich, A.M. Emelyanenko, K.A. Emelyanenko, A.G. Domantovsky, Shiryaev, comment on nanosecond laser textured superhydrophobic metallic surfaces and their chemical sensing applications by Duong V. Ta, Andrew Dunn, Thomas J. Wasley, Robert W. Kay, Jonathan Stringer, Patrick J. Smith, Colm Connaughton, Jonathan D. Shephard, Appl. Surf. Sci. 379 (2016) 111–113. 357 (2015) 248–254), Al. Surf. Sci..
[28] J.Y. Long, M.L. Zhong, P.X. Fan, D.W. Gong, H.J. Zhang, Wettability conversion of ultrafast laser structured copper surface, J. Laser Appl. 27 (2015) S29107, http://dx.doi.org/10.2351/1.4906477.
[29] F.M. Chang, S.L. Cheng, S.J. Hong, Y.J. Sheng, H.K. Tsao, Superhydrophilicity to superhydrophobicity transition of CuO nanowire films, Appl. Phys. Lett. 96 (2010).
[30] P. Bizi-bandoki, S. Valette, E. Audouard, S. Benayoun, Time dependency of the hydrophilicity and hydrophobicity of metallic alloys subjected to femtosecond laser irradiations, Appl. Surf. Sci. 273 (2013) 399–407.
[31] D.V. Ta, A. Dunn, T.J. Wasley, R.W. Kay, J. Stringer, P.J. Smith, C. Connaughton, J.D. Shephard, Nanosecond laser textured superhydrophobic metallic surfaces and their chemical sensing applications, Appl. Surf. Sci. A 357 (2015) 248–254.
[32] M.C. Sharp, A.P. Rosowski, P.W. French, Nanosecond laser texturing of aluminium for control of wettability, Proc. Spie 9657 (2015).
[33] M. Finšgar, I. Milošev, Corrosion behaviour of stainless steels in aqueous solutions of methane sulfonic acid, Corros. Sci. 52 (2010) 2430–2438.
[34] U. Trdan, J. Grum, SEM/EDS characterization of laser shock peening effect on localized corrosion of Al alloy in a near natural chloride environment, Corros. Sci. 82 (2014) 328–338.
[35] C.T. Kwok, K.H. Lo, W.K. Chan, F.T. Cheng, H.C. Man, Effect of laser surface melting on intergranular corrosion behaviour of aged austenitic and duplex stainless steels, Corros. Sci. 53 (2011) 1581–1591.
[36] R.K. Gupta, N. Birbilis, The influence of nanocrystalline structure and processing route on corrosion of stainless steel: a review, Corros. Sci. 92 (2015) 1–15.
[37] P.A. Schweitzer, Fundamentals of Metallic Corrosion, CRC Press, 2007, p. 153.
[38] J. Jiang, D. Xu, T. Xi, M. Babar Shahzad, M. Saleem Khan, J. Zhao, X. Fan, C. Yang, T. Gu, K. Yang, Effects of aging time on intergranular and pitting corrosion behaviour of Cu-bearing 304 L stainless steel in comparison with 304 L stainless steel, Corros. Sci. 113 (2016) 46–56.
[39] Z. Wang, P. Chen, H. Li, B. Fang, R. Song, Z. Zheng, The intergranular corrosion susceptibility of 2024 Al alloy during re–ageing after solution treating and cold–rolling, Corros. Sci. 114 (2017) 156–168.